



HAL
open science

Quasidegenerate ice manifold in a purely two-dimensional square array of nanomagnets

Yann Perrin, Benjamin Canals, Nicolas Rougemaille

► **To cite this version:**

Yann Perrin, Benjamin Canals, Nicolas Rougemaille. Quasidegenerate ice manifold in a purely two-dimensional square array of nanomagnets. *Physical Review B*, 2019, 99 (22), pp.224434. 10.1103/PhysRevB.99.224434 . hal-02358163

HAL Id: hal-02358163

<https://hal.science/hal-02358163>

Submitted on 11 Aug 2023

HAL is a multi-disciplinary open access archive for the deposit and dissemination of scientific research documents, whether they are published or not. The documents may come from teaching and research institutions in France or abroad, or from public or private research centers.

L'archive ouverte pluridisciplinaire **HAL**, est destinée au dépôt et à la diffusion de documents scientifiques de niveau recherche, publiés ou non, émanant des établissements d'enseignement et de recherche français ou étrangers, des laboratoires publics ou privés.

Quasidegenerate ice manifold in a purely two-dimensional square array of nanomagnets

Yann Perrin, Benjamin Canals, and Nicolas Rougemaille

Université Grenoble Alpes, CNRS, Grenoble INP, Institut NEEL, 38000 Grenoble, France

(Received 18 January 2019; revised manuscript received 29 May 2019; published 28 June 2019)

We investigate numerically the low-energy properties of an artificial square spin system in which the nanomagnets are physically connected at the lattice vertex sites. Micromagnetic simulations performed on a single square vertex reveal that type-II vertices always have the lowest energy, in sharp contrast with what is found in lattices made of disconnected nanomagnets, for which type-I vertices are the ground-state configuration. The micromagnetic simulations also show that the energy stored at the vertex sites strongly depends on the type of magnetic domain wall formed by the four connected nanomagnets. Interestingly, the energy gap between type-I and type-II vertices can be drastically reduced by varying the geometrical parameters of the nanomagnets, such as their width and thickness. For typical widths and thicknesses achievable experimentally, we find that this energy gap is small enough to consider type-I and type-II vertices as quasidegenerate. Based on the vertex energies provided by the micromagnetic simulations, we compute the thermodynamic properties of the corresponding spin model using Monte Carlo simulations. In some cases, these properties are hardly distinguishable from those of the celebrated square ice model. Our findings then suggest that an ice physics, characterized by a massively degenerate ground-state manifold at low temperature, may be observed experimentally in a simple square lattice of connected magnetic elements. This work thus provides a route to fabricate artificial algebraic spin liquids using a purely two-dimensional geometry.

DOI: [10.1103/PhysRevB.99.224434](https://doi.org/10.1103/PhysRevB.99.224434)**I. INTRODUCTION**

Artificial arrays of interacting nanomagnets were introduced [1–3] as a mean to fabricate experimentally various types of spin and vertex models. In particular, the idea of using lithographically patterned architectures to explore the physics of highly frustrated magnets [4] triggered a wealth of studies at the frontier between nanomagnetism and condensed matter magnetism. Classical spin liquids [5–7], emerging magnetic properties [7–13], Coulomb phases [14–16] and complex magnetic ordering [17–19] are examples of the low-energy physics that can be now probed experimentally, in an almost routine fashion. Because almost any type of two-dimensional (2d) geometry can be designed, whether or not this geometry exists in nature [20–24], artificial spin systems offer a powerful lab-on-chip approach to directly visualize exotic magnetic phenomena in real space [25,26].

Among the works done so far, the square geometry has been extensively studied [3,27–36]. One reason is that the square geometry potentially allows investigation of ice-type models, a family of vertex models introduced in the thirties by Linus Pauling to describe the residual entropy of water ice at low temperature [37]. However, due to the nonequivalent strengths of the magnetostatic interaction between orthogonal and collinear elements in artificial 2d square arrays of disconnected nanomagnets, these systems were not able to reach the square ice physics. Instead, these arrays order in a Néel-like fashion at low effective temperature, and the macroscopic degeneracy of the ground-state manifold initially sought is lost [3].

However, an extensive degeneracy of the ground-state manifold can be restored if the square geometry is modified.

For example, the Shakti lattice provides means to address the physics of the square ice, but in an emergent form [20,38]. An ice physics may be also recovered if extra nanomagnets are inserted at the vertex sites of the square lattice [15], or if one of the two sublattices is shifted vertically [14,16,27]. These works suggest that experimental tricks have to be used if one wants to counter-balance the nonequivalent strengths of the magnetostatic interaction between orthogonal and collinear nearest neighbors in a square lattice. The question then arises whether an ice physics may be observed in a conventional, two-dimensional square lattice of interacting nanomagnets.

The purpose of this work is to show numerically that an ice manifold can indeed be found in a purely 2d square lattice. To do so, we consider a square array of nanomagnets that extend up to the vertex, meaning that the nanomagnets are physically connected at the nodes of the lattice. Connected square spin systems are then reminiscent of several other works done in the past on magnetic antidot arrays [39–44]. Besides the magnetostatic interaction, the micromagnetic exchange interaction, absent when the nanomagnets are physically disconnected, now plays a key role. Competition between these two interactions generates different micromagnetic textures at the vertex sites, depending on how magnetization is locally oriented. The energy associated with this magnetization distribution is calculated using micromagnetic simulations, and computed as a function of the geometrical parameters of the nanomagnets. Contrarily to what is found when the nanomagnets are disconnected, type-II vertices always have the lowest micromagnetic energy. Moreover, the energy gap between type-I and type-II vertices can be significantly reduced when the width and thickness of the nanomagnets are increased. These findings have two important consequences.

First, the ground-state manifold of an artificial square spin system made of connected nanomagnets is predicted to be extensively degenerate and made of essentially independent, ferromagnetic lines crossing the whole lattice. This is strikingly different from what is observed in otherwise similar lattices made of disconnected nanomagnets. Secondly, as the energy gap between type-I and type-II vertices is reduced, the low-energy configurations of an artificial square spin system with connected elements resemble the ones of the square ice. Otherwise said, the system is predicted to behave at low temperatures as a classical spin liquid. To support these claims, Monte Carlo simulations were performed using an Ising spin Hamiltonian for which the coupling strengths are derived directly from the micromagnetic vertex energies. The low-energy magnetic structure factor is then computed and compared to the one expected in the square ice model. When the energy gap between type-I and type-II vertices is low enough, the magnetic structure factor is hardly distinguishable from the one of the square ice, suggesting that an icelike physics should be observed in a conventional, purely 2d square geometry with connected magnetic elements.

In the next section, we recall the main features of the six vertex model we address in this work. Using micromagnetic simulations performed on a single vertex made of four connected elements, we show in Sec. III that the magnetization distribution at the vertex sites resembles magnetic domain walls in many ways. Their micromagnetic energy is then computed as a function of the width and thickness of the nanomagnets. To describe the associated physics at the scale of a lattice, Monte Carlo simulations are performed using an Ising spin Hamiltonian, and using the previously calculated micromagnetic energies as an input to define the spin-spin coupling strengths. The main result of these Monte Carlo simulations, reported in Sec. IV, is the observation of magnetic correlations that strongly resemble those expected in the square ice model in a finite temperature range. Finally, the advantages and limitations of using artificial square spin systems with connected nanomagnets to reach an ice physics are discussed in Sec. V.

II. THE SIX VERTEX MODEL

In the six vertex model, each local configuration is defined by the state of four arrows (Ising spins) located on the bonds of a square lattice. Among the $2^4 = 16$ possibilities to define a vertex, only the six states made of two spins pointing inwards and two spins pointing outwards the vertex are considered in this model. In other words, only vertices having the lattice equivalent of a divergence-free state are taken into account, while states breaking the divergence-free condition (often called type-III and type-IV vertices) are not considered. These six states are represented in Fig. 1(a) and can have six different energies. Because of symmetry, in artificial arrays of nanomagnets the conditions $E_1 = E_2 = E_I$ and $E_3 = E_4 = E_5 = E_6 = E_{II}$ are fulfilled, such that the six vertices can be sorted in two groups only [see dashed rectangles in Fig. 1(a)]: type-I vertices, with no net magnetic moment, and type-II vertices carrying a nonzero magnetic moment.

We emphasize that the six vertex model is a short-range model, i.e., neighboring vertices do not interact. When an

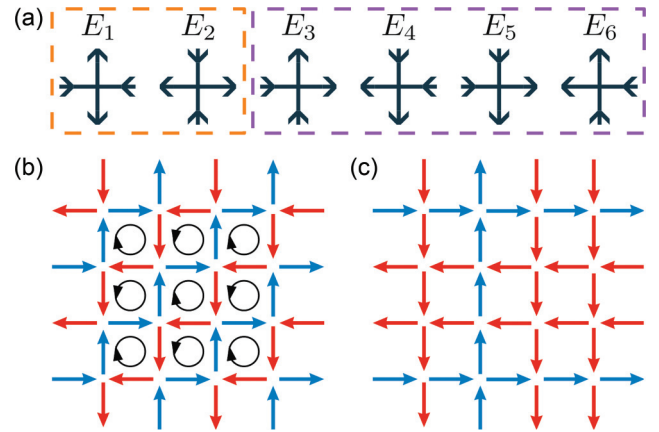


FIG. 1. (a) Schematics of the vertices involved in the six vertex model with their associated energy E . Because of symmetry, these vertices can be sorted in two types only (see dashed rectangles), with $E_1 = E_2 = E_I$ and $E_3 = E_4 = E_5 = E_6 = E_{II}$. (b). Ground-state configuration when $E_I < E_{II}$. (c) One given configuration belonging to the degenerate ground-state manifold when $E_I > E_{II}$.

artificial spin system is described by the six vertex model, one implicitly assumes that the nanomagnets are coupled through first neighbor interaction only. In the following, we consider that the long-range magnetostatic interaction can be neglected. The impact of the dipolar interaction on the ground-state degeneracy will be discussed in Sec. V.

In artificial 2d arrays of disconnected nanomagnets, magnetostatics leads to the condition $E_I < E_{II}$. This condition implies that the low-energy physics of these arrays is described by the F model: [45,46] the magnetic ground state is antiferromagnetically ordered, and consists of flux-closure loops with alternating chirality [see Fig. 1(b)]. Artificial spin systems can be also designed in such a way that the condition $E_I = E_{II}$ is fulfilled [14,16,27]. In that case, the low-energy physics of the array is described by the square ice model [47] and the ground-state manifold is macroscopically degenerate. The magnetic system is an algebraic spin liquid, i.e., a spin liquid characterized by spin-spin correlations decaying as a power law with the separating distance [14]. Local configurations breaking the divergence-free constraint associated with the six vertex model behave, in that particular case, and in that particular case only, as deconfined particulelike excitations interacting via a Coulomb potential [48,49], the so-called classical magnetic monopoles.

In the following, we consider the third possible situation of the six vertex model in which $E_I > E_{II}$. The low-energy physics of the system is then described by the KDP model [50,51] initially introduced to describe ferroelectrics. In that case, the ground state is extensively degenerate and made of decoupled ferromagnetic lines crossing the entire lattice [see Fig. 1(c)]. In the next section, we will show that considering a vertex made of four physically connected elements necessarily leads to the condition $E_I > E_{II}$, thus offering a mean to fabricate experimentally a KDP system. We will also show that the energy difference $E_I - E_{II} > 0$ can be made small enough to consider the limit case where the low-energy physics of the KDP model is difficult to distinguish from a square ice manifold.

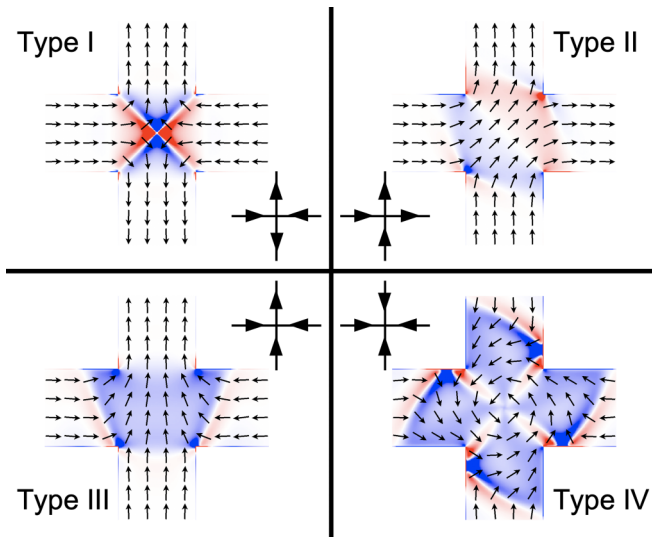


FIG. 2. Micromagnetic configurations of type-I, II, III, and IV vertices for 200-nm-wide, 20-nm-thick permalloy nanomagnets. Small black arrows represent the direction of magnetization within the nanomagnets, while the blue/red contrast codes for the divergence of the magnetization vector.

III. MICROMAGNETIC SIMULATIONS

We examine the micromagnetic energy of a single square vertex. The energy is computed for the four vertex types as a function of the width and thickness of the nanomagnets. The main purpose here is to show that the micromagnetic energy of type-I and type-II vertices can reach similar values, provided that the thickness and width of the nanomagnets are chosen appropriately. As mentioned above, since the condition $E_I = E_{II}$ is required to restore an extensive degeneracy of the ground-state manifold, this result suggests that a low-energy icelike physics might be present in square lattices with connected nanomagnets.

The micromagnetic simulations were performed using the OOMMF code from NIST [52]. The mesh size was set to $2 \times 2 \times t \text{ nm}^3$, where t is the thickness of the nanomagnets. Spontaneous magnetization M_s and exchange stiffness A are those of permalloy: $\mu_0 M_s = 1.0053 \text{ T}$, $A = 10 \text{ pJ/m}$, while magnetocrystalline anisotropy is neglected. We assume that these parameters, especially M_s , are constant all over the range of thicknesses probed in this work. We thus neglect possible changes in the M_s value when the nanomagnets become atomically thin. In all the simulations we performed, the nanomagnets are uniformly magnetized and the magnetic moments at the extremities of the nanomagnets are fixed to avoid nonuniform magnetization profiles at the edges. The magnetization is then nonuniform only at the vertex site and we exclude here multidomain configurations within the nanomagnets that might occur experimentally (see the discussion in Sec. V).

The micromagnetic configurations for the four vertex types are reported in Fig. 2. Since the nanomagnets are connected, these configurations are similar to magnetic domain walls in many ways. Type-I vertices have the form of a magnetic antivortex [53], while type-II vertices are almost homogeneously

magnetized in (11)-like directions. Type-III vertices have the form of a transverse domain wall separating the two horizontal head-to-head nanomagnets. Type-IV vertices resemble a vortex domain wall, with an anticlockwise chirality in Fig. 2.

The energetics of magnetic domain walls usually depends on the geometrical parameters of the nanostructure. We then changed the geometrical parameters of the nanomagnets in a wide range of width [50–400] and thickness [0.5–40], where numbers are in nanometers. Figure 3 shows how the total micromagnetic energy of each vertex type varies as a function of those parameters. These numerical results have two main consequences regarding the type of model that can be potentially accessed experimentally using a square lattice of connected nanomagnets.

First, in the whole range of parameters explored here, type-II vertices have the lowest energy (see red curves in Fig. 3). Therefore the ground-state configuration consists of independent ferromagnetic lines crossing the entire network [see Fig. 1(c)], as predicted by the KDP model. This is in sharp contrast with artificial square spin systems made of disconnected nanomagnets in which type-I vertices have always the lowest energy, leading to a twofold degenerate ground state made of local flux-closure configurations [see Fig. 1(b)]. Therefore a new model can be reached simply by connecting the nanomagnets in a 2d square lattice. We emphasize that the ground-state manifold associated with this model is extensively degenerate, although this degeneracy is subdominant (i.e., the entropy per spin tends to zero at the thermodynamic limit when the temperature approaches zero, even though the degeneracy of the ground-state manifold is extensive).

The second consequence deduced from Fig. 3 is the capability to obtain a quasi-ice condition ($E_I \approx E_{II}$) as type-I and type-II vertices asymptotically tend to the same energy in the limit of thick and/or wide nanomagnets. Clearly, type-II vertices have still the lowest energy, but for large thicknesses (30–40 nm) and reasonable width (200 nm or more), we can envision that sample defects or thermal fluctuations for example will allow the system to select both vertex types equivalently. This might offer a unique opportunity to probe a low-energy icelike physics in a purely two-dimensional square array of connected nanomagnets.

IV. THERMODYNAMIC PROPERTIES

We now examine the thermodynamic properties of the spin model associated with the micromagnetic properties described above. To do so, Monte Carlo simulations were performed using the Hamiltonian $H = -J_1 \sum_{\langle ij \rangle} \sigma_i \cdot \sigma_j - J_2 \sum_{\langle\langle ij \rangle\rangle} \sigma_i \cdot \sigma_j$, where σ_i and σ_j are Ising variables on sites i and j . J_1 and J_2 are positive coupling strengths between orthogonal and collinear nearest neighbors, respectively. The simulations were done for a $20 \times 20 \times 2$ site lattice with periodic boundary conditions. A single spin flip algorithm was used to capture the physics that might be observed experimentally, where local magnetization reversal is the only relevant dynamics. As a consequence, the simulations suffer from a critical slowing down when approaching the ground-state manifold. At low temperatures, the system freezes, as that would be the case experimentally. The cooling procedure

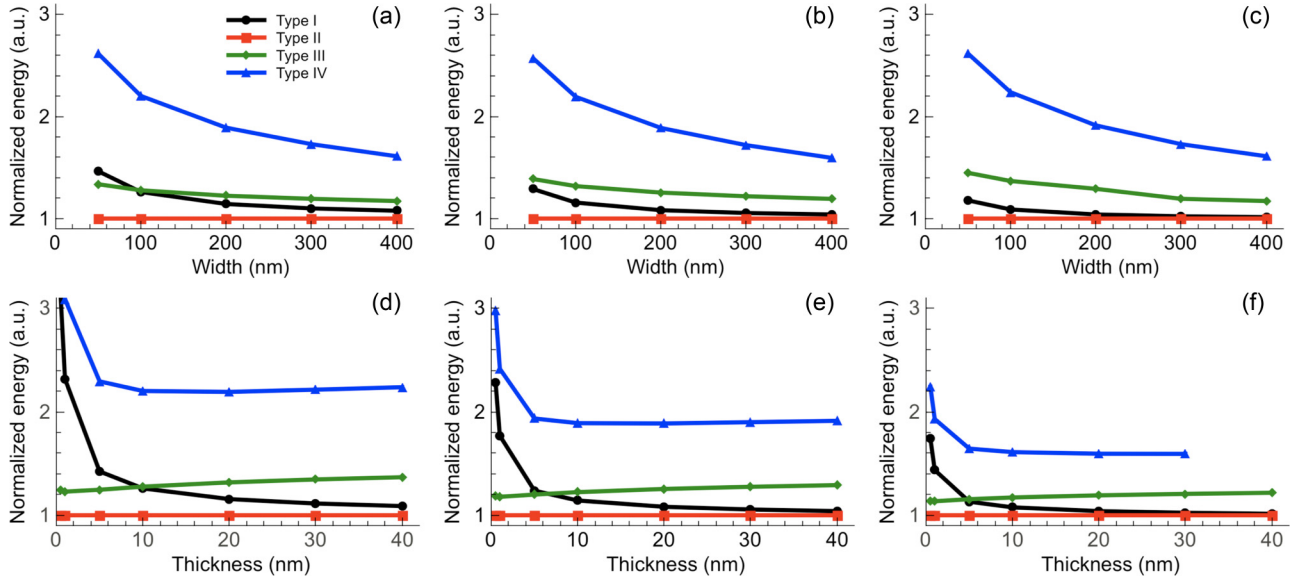


FIG. 3. Normalized micromagnetic energy of the four vertex types as a function of the width and thickness of the nanomagnets. Nanomagnets are 10-, 20-, and 40-nm-thick in (a)–(c), respectively, while they are 100-, 200-, and 400-nm-wide in (d)–(f), respectively. Type-II vertices have always the lowest energy, which is taken here as the reference energy. a.u., arbitrary units.

starts from $T/J_1 = 100$ and ends at $T/J_1 = 0.1$. 10^4 modified Monte Carlo steps (mmcs) are used for thermalization [54]. Measurements follow the thermalization and are computed also with 10^4 mmcs.

The coupling strengths J_1 and J_2 used in the Monte Carlo simulations are directly derived from the micromagnetic energies calculated in the previous section. To do so, we link the micromagnetic energy E_{DW_i} of a domain wall [with $i = (1, \dots, 4)$ for type i vertices] to the coupling strengths J_1 and J_2 using the following equations:

$$\begin{aligned} E_{DW_1} &= -4J_1 + 2J_2, \\ E_{DW_2} &= -2J_2, \\ E_{DW_3} &= 0, \\ E_{DW_4} &= 4J_1 + 2J_2. \end{aligned} \quad (1)$$

Although these equations provide the correspondence between the two approaches, E_{DW_i} is not directly computed in our OOMMF simulations. Instead, we compute the total micromagnetic energy of a vertex made of four connected nanomagnets, which is the sum of all four internal energies E_0 plus the energy of the domain wall formed at the vertex site. We emphasize that, contrarily to a spin in a spin model, a nanomagnet has an internal energy E_0 , which is a function of its thickness and width.

The total micromagnetic energy of the type i vertex can be represented as $E_i = 4E_0 + E_{DW_i}$. Considering the first three energies E_1 , E_2 , and E_3 , we get

$$\frac{E_1 - E_3}{E_2 - E_3} = 2 \frac{J_1}{J_2} - 1 \quad (2)$$

or

$$\frac{E_2 - E_4}{E_1 - E_4} = \frac{1}{2} \left(\frac{J_2}{J_1} + 1 \right) \quad (3)$$

if we consider E_1 , E_2 , and E_4 . The ratio J_2/J_1 is thus determined from the micromagnetic energies of the different vertex types. Fixing J_1 to 1, J_2 is calculated from Eq. (2) or (3) (both equations give similar results).

The spin-spin correlations deduced from the real space configurations are Fourier transformed for all computed temperatures, leading to a magnetic structure factor. We define the magnetic structure factor as in neutron scattering experiments, where the spin correlations perpendicular to the diffusion vector are measured [14]. It is composed of a matrix of 81×81 points covering an area of $\pm 6\pi$ along the q_x and q_y directions in reciprocal space.

The magnetic structure factors obtained at the lowest sampled temperatures are reported in Fig. 4 for different J_2 values. As expected, when $J_2 = 1$, we find the magnetic structure factor of the square ice, characteristic of an algebraic spin liquid with its associated pinch points [14]. For J_2 values larger than 1.1, the magnetic structure factor is drastically different and made of lines spanning across the reciprocal space, consistently with the formation of decoupled ferromagnetic lines in real space. More importantly, for J_2 values up to 1.03 typically, the magnetic structure factor strongly resembles the one of the square ice [see Figs. 4(a)–4(c)]. This is so because the single spin flip dynamics used in the Monte Carlo simulations is unable to reach the ground-state configuration of the KDP model as J_2 approaches J_1 . The low-temperature physics is then similar to the one of the square ice, even though the ground state is different. Otherwise said, although J_2 is not strictly equal to J_1 , it is close enough to push the ground-state configuration of the KDP model down to inaccessible low temperatures. We note that this regime, where J_2/J_1 is smaller than 1.03 is achieved for example for nanomagnets having a width of 400 nm and a thickness of 40 nm [see Fig. 5 where the J_2/J_1 ratio calculated from Eq. (2) is plotted as a function of the width for 20- and 40-nm-thick nanomagnets]. Our results then suggest that connected artificial spin systems

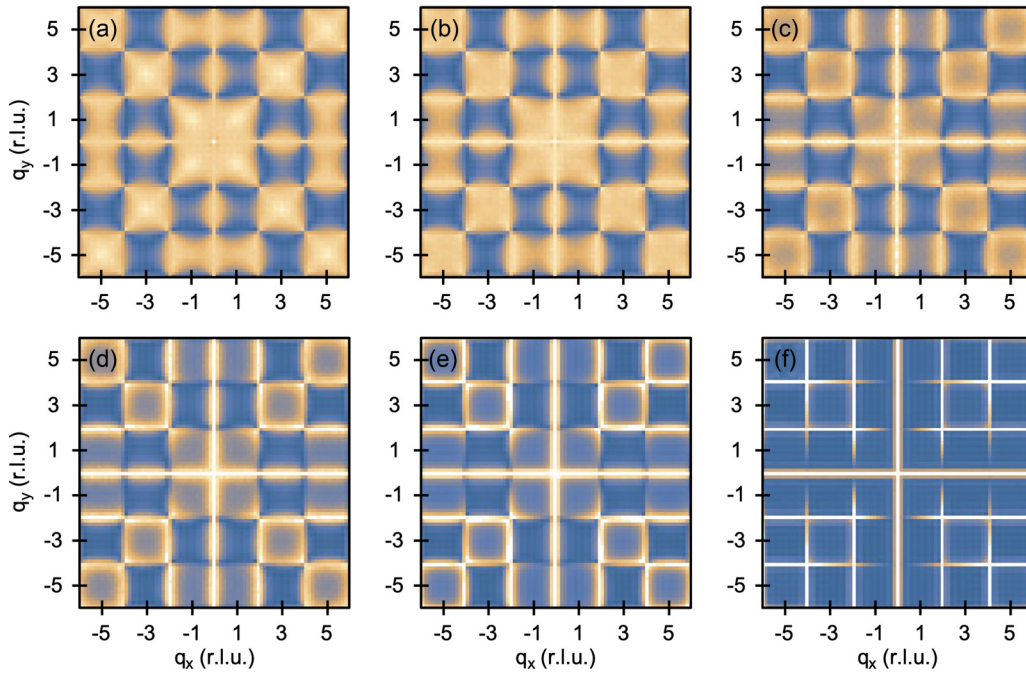


FIG. 4. Computed magnetic structure factors at the lowest sampled temperature for $J_2 = 1$ (a), 1.01 (b), 1.03 (c), 1.05 (d), 1.1 (e), and 1.2 (f). $J_1 = 1$ in all cases. Intensity is normalized the same way in all images. r.l.u., reciprocal lattice unit.

with geometrical parameters easily achievable experimentally should behave similarly to the square ice, i.e., a low-energy, extensively degenerate manifold should be captured experimentally.

V. DISCUSSION

In this section, we discuss the applicability of our numerical findings to potential experiments. In particular, we come back on the assumptions we made throughout our analysis and justify the choice (i) of considering that the nanomagnets are uniformly magnetized between neighboring vertices and (ii) of neglecting the role of long-range interactions between the vertices.

First of all, the results described above show that the micromagnetic nature of artificial spin systems made of

connected nanomagnets can be used to invert the hierarchy of the type-I and type-II vertex energies in a square lattice. Besides, choosing appropriately the width and thickness of the nanomagnets allows a substantial reduction of the energy gap $E_I - E_{II} > 0$, which tends to vanish in the limit of thick and/or wide magnetic elements. Micromagnetism [55–59], which is usually neglected or avoided in artificial spin ice systems, can be used as an extra knob to restore an icelike physics in a conventional, easy-to-implement two-dimensional lattice. Based on our Monte Carlo simulations, we find that J_2 must be smaller than $1.03 \times J_1$ to approach an ice physics at very low temperature. However, we expect in practice the low-energy physics of artificial arrays of connected nanomagnets to be hardly distinguishable from an icelike system even for less restrictive conditions on the J_2/J_1 ratio.

Indeed, the comparison we made above between the magnetic structure factor of the square ice and the one expected when the $J_2 = J_1$ condition is slightly detuned has been done for a large averaging (what is reported in Fig. 4 is an average of 10^4 measurements at low temperatures). In practice, a few snapshots only will be available experimentally and the effective temperature that can be reached through a demagnetization protocol or a thermal annealing will remain fairly large (of the order of the coupling strength J) [14–16]. Otherwise said, given the intrinsic signal to noise ratio accessible experimentally, the J_2/J_1 value might be further increased while still preserving a magnetic structure factor similar to the one expected in the square ice model. The impact of the temperature can be illustrated by comparing the simulated magnetic structure factors at a temperature $T/J_1 = 1$ for several J_2/J_1 ratios (see Fig. 6). Such a comparison reveals only small differences between the square ice [$J_2 = J_1$, see Fig. 6(a)] and a KDP model for which $J_2/J_1 = 1.1$ [see Fig. 6(c)]. In particular, the magnetic structure factor

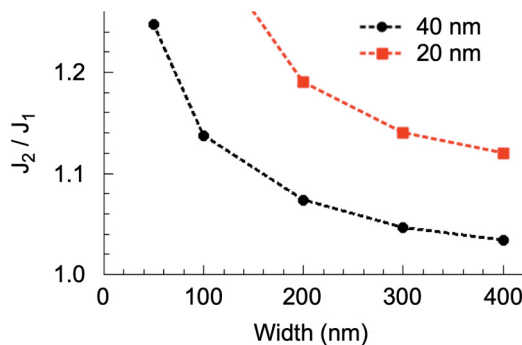


FIG. 5. Ratio between the J_2 and J_1 coupling strengths deduced from the micromagnetic vertex energies as a function of the width of the nanomagnets. Red squares and black dots correspond to a thickness of 20 and 40 nm, respectively.

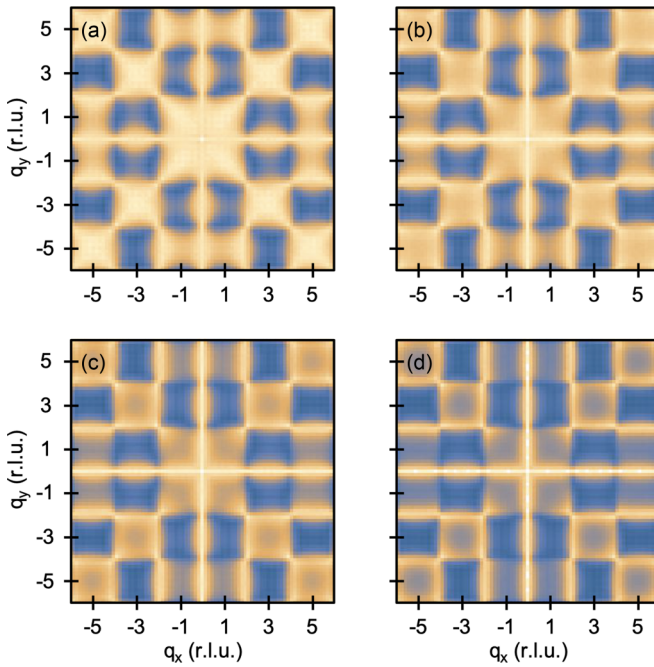


FIG. 6. Computed magnetic structure factors at the effective temperature $T/J_1 = 1$ for $J_2/J_1 = 1$ (a), 1.05 (b), 1.10 (c), and 1.15 (d). Intensity is normalized the same way in all images. r.l.u., reciprocal lattice unit.

is still diffuse but structured in the latter case, and strongly resembles the one of an algebraic spin liquid. The interest here is the less restrictive J_2/J_1 condition required experimentally, which allows to envision the design of artificial arrays with nanomagnets having a width of 200 nm or less, and a thickness of 40 nm (see Fig. 5).

This is an important point as in our micromagnetic description we neglected the possibility to have nanomagnets with a multidomain configuration and we assumed that the magnetization always remains uniform along the long axis of the elements. This approximation is questionable, especially in the limit of large and thick nanomagnets. For example, it is likely experimentally that 400-nm-wide and 40-nm-thick nanomagnets tend to have a multidomain state when properly field demagnetized or thermally activated. However, the observation of an icelike magnetic structure factor at $T/J_1 = 1$ for $J_2/J_1 = 1.1$ suggests that the quasidegeneracy we found is valid for width of 200 nm or less, for which experiments show a single domain configuration [60].

We also envision that it would be more promising to test our predictions using a thermally active spin system rather than an athermal one subject to a field demagnetization

protocol. The reason is that field driven protocols will likely propagate efficiently magnetic domain walls throughout the lattice, thus favoring the formation of type-II vertices. Such kinetic effects might be less pronounced in thermally active systems annealed above the Curie point of the consistent material.

Finally, as mentioned in Sec. II, we have considered so far that artificial spin systems consisting of connected nanomagnets are well approximated by a short-ranged spin model. This approximation is also questionable as artificial arrays of nanomagnets are known to be dipolar by nature [5,7,17,26]. However, the short-range approximation works well for the square ice geometry and the low-energy manifold imaged in disconnected arrays of nanomagnets shows no trace of dipolar signatures [14,16]. One possible explanation is that the square ice model becomes a loop model in its low-energy manifold, i.e., the relevant excitations once the ice rule is obeyed everywhere are collective loop moves [26]. Experimentally, the only relevant spin dynamics involves single spin flip events, but this dynamics encounters a critical slowing down when the system enters an ice regime. Consequently, whatever the experimental protocol used to lower the system energy, whether it is a field demagnetization protocol [14] or a thermal annealing [16], the system freezes way before the long-range dipolar interactions can lift the energy degeneracy. Although dipolar by nature, artificial square ice systems are then well described by a short-range spin Hamiltonian. Note that this behavior is very similar to the one of the three-dimensional condensed matter pyrochlore dipolar spin ices. There, dynamical freezing can be an issue as it prevents observing the expected ordered ground state, or an advantage, as it allows to observe the emergent physics of a three-dimensional Coulomb phase on a finite temperature range [61]. Besides this dynamical reason, the long-range dipolar interaction can always be made negligible by increasing the length of the nanomagnets. Since the energy that matters is the micromagnetic energy stored at the vertex sites, one can imagine to design lattices consisting of nanomagnets with large aspect ratios. In fact, fabricating a series of connected lattices with various aspect ratios, while keeping the width and thickness unchanged, might be a powerful way to understand to what extent the vertex-vertex interaction can be neglected. However, for the purpose of restoring an icelike degeneracy, long nanomagnets can be easily fabricated.

ACKNOWLEDGMENT

This work was supported by the Agence Nationale de la Recherche through project No. ANR12-BS04-009 “Frustrated.”

- [1] M. Tanaka, E. Saitoh, H. Miyajima, T. Yamaoka, and Y. Iye, *J. Appl. Phys.* **97**, 10J710 (2005).
- [2] M. Tanaka, E. Saitoh, H. Miyajima, T. Yamaoka, and Y. Iye, *Phys. Rev. B* **73**, 052411 (2006).
- [3] R. F. Wang, C. Nisoli, R. S. Freitas, J. Li, W. McConville, B. J. Cooley, M. S. Lund, N. Samarth, C. Leighton, V. H. Crespi, and P. Schiffer, *Nature (London)* **439**, 303 (2006).

- [4] *Introduction to Frustrated Magnetism*, edited by C. Lacroix, P. Mendels, and F. Mila, Springer Series in Solid State Sciences Vol. 164 (Springer, New York, 2011).
- [5] Y. Qi, T. Brintlinger, and J. Cumings, *Phys. Rev. B* **77**, 094418 (2008).
- [6] O. Sendetskyi, L. Anghinolfi, V. Scagnoli, G. Möller, N. Leo, A. Alberca, J. Kohlbrecher, J. Lüning, U. Staub, and L. J. Heyderman, *Phys. Rev. B* **93**, 224413 (2016).

- [7] N. Rougemaille, F. Montaigne, B. Canals, A. Duluard, D. Lacour, M. Hehn, R. Belkhou, O. Fruchart, S. El Moussaoui, A. Bendouan, and F. Maccherozzi, *Phys. Rev. Lett.* **106**, 057209 (2011).
- [8] G. Möller and R. Moessner, *Phys. Rev. B* **80**, 140409(R) (2009).
- [9] S. Zhang, I. Gilbert, C. Nisoli, G.-W. Chern, M. J. Erickson, L. O'Brien, C. Leighton, P. E. Lammert, V. H. Crespi, and P. Schiffer, *Nature (London)* **500**, 553 (2013).
- [10] I. A. Chioar, B. Canals, D. Lacour, M. Hehn, B. Santos Burgos, T. O. Menteş, A. Locatelli, F. Montaigne, and N. Rougemaille, *Phys. Rev. B* **90**, 220407(R) (2014).
- [11] F. Montaigne, D. Lacour, I. A. Chioar, N. Rougemaille, D. Louis, S. M. Murtry, H. Riahi, B. S. Burgos, T. O. Menteş, A. Locatelli, B. Canals, and M. Hehn, *Sci. Rep.* **4**, 5702 (2014).
- [12] M. E. Brooks-Bartlett, S. T. Banks, L. D. C. Jaubert, A. Harman-Clarke, and P. C. W. Holdsworth, *Phys. Rev. X* **4**, 011007 (2014).
- [13] B. Canals, I. A. Chioar, V. D. Nguyen, M. Hehn, D. Lacour, F. Montaigne, A. Locatelli, T. O. Menteş, B. Santos Burgos, and N. Rougemaille, *Nat. Commun.* **7**, 11446 (2016).
- [14] Y. Perrin, B. Canals, and N. Rougemaille, *Nature (London)* **540**, 410 (2016).
- [15] E. Östman, H. Stopfel, I.-A. Chioar, U. B. Arnalds, A. Stein, V. Kapaklis, and B. Hjörvarsson, *Nat. Phys.* **14**, 375 (2018).
- [16] A. Farhan, M. Saccone, C. F. Petersen, S. Dhuey, R. V. Chopdekar, Y.-L. Huang, N. Kent, Z. Chen, M. J. Alava, T. Lippert, A. Scholl, and S. van Dijken, *Sci. Adv.* **5**, eaav6380 (2019).
- [17] I. A. Chioar, N. Rougemaille, A. Grimm, O. Fruchart, E. Wagner, M. Hehn, D. Lacour, F. Montaigne, and B. Canals, *Phys. Rev. B* **90**, 064411 (2014).
- [18] I. A. Chioar, N. Rougemaille, and B. Canals, *Phys. Rev. B* **93**, 214410 (2016).
- [19] J. Hamp, R. Moessner, and C. Castelnovo, *Phys. Rev. B* **98**, 144439 (2018).
- [20] I. Gilbert, G.-W. Chern, S. Zhang, L. O'Brien, B. Fore, C. Nisoli, and P. Schiffer, *Nat. Phys.* **10**, 670 (2014).
- [21] I. Gilbert, Y. Lao, I. Carrasquillo, L. O'Brien, J. D. Watts, M. Manno, C. Leighton, A. Scholl, C. Nisoli, and P. Schiffer, *Nat. Phys.* **12**, 162 (2015).
- [22] H. Stopfel, E. Östman, I.-A. Chioar, D. Greving, U. B. Arnalds, T. P. A. Hase, A. Stein, B. Hjörvarsson, and V. Kapaklis, *Phys. Rev. B* **98**, 014435 (2018).
- [23] D. Shi, Z. Budrikis, A. Stein, S. A. Morley, P. D. Olmsted, G. Burnell, and C. H. Marrows, *Nat. Phys.* **14**, 309 (2018).
- [24] M. J. Morrison, T. R. Nelson, and C. Nisoli, *New J. Phys.* **15**, 045009 (2013).
- [25] C. Nisoli, R. Moessner, and P. Schiffer, *Rev. Mod. Phys.* **85**, 1473 (2013).
- [26] N. Rougemaille and B. Canals, *Eur. Phys. J. B* **92**, 62 (2019).
- [27] G. Möller and R. Moessner, *Phys. Rev. Lett.* **96**, 237202 (2006).
- [28] C. Nisoli, J. Li, X. L. Ke, D. Garand, P. Schiffer, and V. H. Crespi, *Phys. Rev. Lett.* **105**, 047205 (2010).
- [29] J. P. Morgan, A. Stein, S. Langridge, and C. H. Marrows, *Nat. Phys.* **7**, 75 (2011).
- [30] C. Phatak, A. K. Petford-Long, O. Heinonen, M. Tanase, and M. De Graef, *Phys. Rev. B* **83**, 174431 (2011).
- [31] Z. Budrikis, P. Politi, and R. L. Stamps, *Phys. Rev. Lett.* **107**, 217204 (2011).
- [32] Z. Budrikis, K. L. Livesey, J. P. Morgan, J. Akerman, A. Stein, S. Langridge, C. H. Marrows, and R. L. Stamps, *New J. Phys.* **14**, 035014 (2012).
- [33] A. Farhan, P. M. Derlet, A. Kleibert, A. Balan, R. V. Chopdekar, M. Wyss, J. Perron, A. Scholl, F. Nolting, and L. J. Heyderman, *Phys. Rev. Lett.* **111**, 057204 (2013).
- [34] J. M. Porro, A. Bedoya-Pinto, A. Berger, and P. Vavassori, *New J. Phys.* **15**, 055012 (2013).
- [35] V. Kapaklis, U. B. Arnalds, A. Farhan, R. V. Chopdekar, A. Balan, A. Scholl, L. J. Heyderman, and B. Hjörvarsson, *Nat. Nanotech.* **9**, 514 (2014).
- [36] D. Thonig, S. Reißaus, I. Mertig, and J. Henk, *J. Phys.: Condens. Matter* **26**, 266006 (2014).
- [37] L. Pauling, *J. Am. Chem. Soc.* **57**, 2680 (1935).
- [38] G.-W. Chern, M. J. Morrison, and C. Nisoli, *Phys. Rev. Lett.* **111**, 177201 (2013).
- [39] C. T. Yu, H. Jiang, L. Shen, P. J. Flanders, and G. J. Mankey, *J. Appl. Phys.* **87**, 6322 (2000).
- [40] P. Vavassori, G. Gubbiotti, G. Zangari, C. T. Yu, H. Yin, H. Jiang, and G. J. Mankey, *J. Appl. Phys.* **91**, 7992 (2002).
- [41] C. C. Wang, A. O. Adeyeye, and Y. H. Wu, *J. Appl. Phys.* **94**, 6644 (2003).
- [42] I. Guedes, M. Grimsditch, V. Metlushko, P. Vavassori, R. Camley, B. Ilic, P. Neuzil, and R. Kumar, *Phys. Rev. B* **67**, 024428 (2003).
- [43] L. J. Heyderman, F. Nolting, and C. Quitmann, *Appl. Phys. Lett.* **83**, 1797 (2003).
- [44] T. Schneider, M. Langer, J. Alekhina, E. Kowalska, A. Oelschlägel, A. Semisalova, A. Neudert, K. Lenz, K. Potzger, M. P. Kostylev, J. Fassbender, A. O. Adeyeye, J. Lindner, and R. Bali, *Sci. Rep.* **7**, 41157 (2017).
- [45] F. Rys, *Helv. Phys. Acta* **36**, 537 (1963).
- [46] E. H. Lieb, *Phys. Rev. Lett.* **18**, 1046 (1967).
- [47] E. H. Lieb, *Phys. Rev.* **162**, 162 (1967).
- [48] C. Castelnovo, R. Moessner, and S. L. Sondhi, *Nature (London)* **451**, 42 (2008).
- [49] C. L. Henley, *Annu. Rev. Condens. Matter Phys.* **1**, 179 (2010).
- [50] J. C. Slater, *J. Chem. Phys.* **9**, 16 (1941).
- [51] E. H. Lieb, *Phys. Rev. Lett.* **19**, 108 (1967).
- [52] M. Donahue and D. Porter, Interagency Report NISTIR 6376, National Institute of Standards and Technology, Gaithersburg, MD, 1999.
- [53] V. L. Mironov, O. L. Ermolaeva, S. A. Gusev, A. Yu. Klimov, V. V. Rogov, B. A. Gribkov, O. G. Udalov, A. A. Fraerman, R. Marsh, C. Checkley, R. Shaikhaidarov, and V. T. Petrashov, *Phys. Rev. B* **81**, 094436 (2010).
- [54] One modified Monte Carlo step corresponds to a sequence of spin flip attempts such that, on average, each spin is flipped once. This is mandatory to achieve statistical independence. In practice, this corresponds to a number of trials equal to N (number of sites) \times the inverse of the acceptance rate (average value of the spin flip acceptance). At the lowest temperatures, 10^4 mmscs corresponds typically to 10^8 spin flip trials.
- [55] N. Rougemaille, F. Montaigne, B. Canals, M. Hehn, H. Riahi, D. Lacour, and J.-C. Toussaint, *New J. Phys.* **15**, 035026 (2013).

- [56] D. M. Burn, M. Chadha, S. K. Walton, and W. R. Branford, [Phys. Rev. B **90**, 144414 \(2014\)](#).
- [57] D. M. Burn, M. Chadha, and W. R. Branford, [Phys. Rev. B **92**, 214425 \(2015\)](#).
- [58] S. K. Walton, K. Zeissler, D. M. Burn, S. Ladak, D. E. Read, T. Tyliczszak, L. F. Cohen, and W. R. Branford, [New J. Phys. **17**, 013054 \(2015\)](#).
- [59] S. Gliga, A. Kákay, L. J. Heyderman, R. Hertel, and O. G. Heinonen, [Phys. Rev. B **92**, 060413\(R\) \(2015\)](#).
- [60] V.-D. Nguyen, Y. Perrin, S. Le Denmat, B. Canals, and N. Rougemaille, [Phys. Rev. B **96**, 014402 \(2017\)](#).
- [61] B. C. den Hertog and M. J. P. Gingras, [Phys. Rev. Lett. **84**, 3430 \(2000\)](#).